Eur. Phys. J. A **29**, 307–313 (2006)
DOI 10.1140/epja/i2006-10092-x

THE EUROPEAN PHYSICAL JOURNAL A

Phase motion of baryon resonances

E. Klempt[1,a], A.V. Anisovich[1,2], V.A. Nikonov[1,2], A.V. Sarantsev[1,2], and U. Thoma[1,3]

[1] Helmholtz-Institut für Strahlen- und Kernphysik, Universität Bonn, Germany
[2] Petersburg Nuclear Physics Institute, Gatchina, Russia
[3] Physikalisches Institut, Universität Gießen, Germany

Received: 12 January 2006 / Revised: 11 July 2006 /
Published online: 21 September 2006 –
Communicated by V. Vento

Abstract. A novel technique to probe the resonant structure of a partial-wave amplitude is proposed and applied to data on photoproduction of baryon resonances.

PACS. 11.80.Et Partial-wave analysis – 13.30.-a Decays of baryons – 13.60.Le Meson production – 14.20.Gk Baryon resonances with $S = 0$

1 Introduction

The quest for a better understanding of the high-mass spectrum of baryon resonances and the search for missing resonances are the driving forces behind the intensive studies of photoproduction reactions at several facilities like ELSA (Bonn), GRAAL (Grenoble), JLab (Newport News), MAMI (Mainz), and SPring-8 (Hyogo). The mechanisms which confine quarks are not well understood; the high-mass baryon excitation spectrum seems to be the best place to study quark-quark interactions in the confinement region. However, data on high-mass baryon resonances are scarce. The leading N* resonances with $J = L+1/2$ are known for orbital angular momenta $L \leq 6$. In quark models, many more states are predicted in all partial waves [1–3] which have not been identified. It is, however, difficult to imagine that all the predicted states are realized as individual resonances with specified properties. Possibly, the number of states is reduced by diquark effects [4] but it is unclear how diquark excitations could be frozen. Perhaps, only quark-diquark excitations can be reached in π or photo-produced reactions [5]. Even more exciting, a phase transition may take place in which chiral symmetry is restored [6] (see, however, [7]).

In two previous papers we reported results of a combined analysis of photoproduction experiments with πN, ηN, KΛ, and KΣ final states [8]. The data included CB-ELSA π^0 and η photoproduction data [9,10], the Mainz-TAPS data [11] on η photoproduction, beam-asymmetry measurements of π^0 and η [12–14], data on $\gamma p \to n\pi^+$ [15] and from the compilation of the SAID database [13]. Simultaneously data on photoproduction of $\gamma p \to K^+\Lambda$ and $\gamma p \to K^+\Sigma^0$ from SAPHIR [16,17], CLAS [18,19], and LEPS [20] were used in the analysis. The formalism used to describe the data is documented in [21]. It uses Breit-Wigner amplitudes (or K matrices) to describe resonant contributions, Reggeised amplitudes for t-channel exchanges and includes amplitudes for u-channel exchanges and Born amplitudes.

A good overall fit was achieved; table 1 summarizes the data used and the χ^2 with which the data were described in the final fit. The fits minimized a pseudo-chisquare function

$$\chi^2_{\rm tot} = \frac{\sum w_i \chi^2_i}{\sum w_i\, N_i} \sum N_i, \qquad (1)$$

where the N_i are given as $N_{\rm data}$ (per channel) in the second column and the weights in the fifth column of table 1.

The fit identified contributions from 14N* and 7Δ^* resonances, 4 of them were new, N(1840)P$_{11}$, N(1870)D$_{13}$, N(2070)D$_{15}$ and, with weaker evidence, N(2170)D$_{13}$. These resonances led to a significant improvement in χ^2 for at least two of the reactions and this was the criterium for us to postulate their existence. But further confirmation for all these resonances is certainly needed.

Clearly, this procedure is not fully satisfactory. In an ideal world, a "complete experiment" would be carried out providing data from many independent polarization and double-polarization measurements to allow for a model-independent multipole analysis of single-meson (and multi-meson) photoproduction. The information should then be used to determine amplitudes for each partial wave from which, in a later stage, background contributions and pole positions of contributing resonances could be determined. In practice, experimental limitations (with a finite number of data points, limited statistics, in-

[a] e-mail: klempt@hiskp.uni-bonn.de

Table 1. Data used in the partial-wave analysis, χ^2 contributions and fitting weights.

Observable	$N_{\rm data}$	χ^2	$\chi^2/N_{\rm data}$	Weight	Ref.
$\sigma(\gamma p \to \Lambda K^+)$	720	804	1.12	4	[16]
$\sigma(\gamma p \to \Lambda K^+)$	770	1282	1.67	2	[18]
$P(\gamma p \to \Lambda K^+)$	202	374	1.85	1	[18]
$\Sigma(\gamma p \to \Lambda K^+)$	45	62	1.42	15	[20]
$\sigma(\gamma p \to \Sigma^0 K^+)$	660	834	1.27	1	[16]
$\sigma(\gamma p \to \Sigma^0 K^+)$	782	2446	3.13	1	[18]
$P(\gamma p \to \Sigma^0 K^+)$	95	166	1.76	1	[18]
$\Sigma(\gamma p \to \Sigma^0 K^+)$	45	20	0.46	35	[20]
$\sigma(\gamma p \to \Sigma^+ K^0)$	48	104	2.20	2	[19]
$\sigma(\gamma p \to \Sigma^+ K^0)$	120	109	0.91	5	[17]
$\sigma(\gamma p \to p\pi^0)$	1106	1654	1.50	8	[9]
$\sigma(\gamma p \to p\pi^0)$	861	2354	2.74	3.5	[12]
$\Sigma(\gamma p \to p\pi^0)$	469	1606	3.43	2	[12]
$\Sigma(\gamma p \to p\pi^0)$	593	1702	2.87	2	[13]
$\sigma(\gamma p \to n\pi^+)$	1583	4524	2.86	1	[15]
$\sigma(\gamma p \to p\eta)$	667	608	0.91	35	[10]
$\sigma(\gamma p \to p\eta)$	100	158	1.60	7	[11]
$\Sigma(\gamma p \to p\eta)$	51	114	2.27	10	[14]
$\Sigma(\gamma p \to p\eta)$	100	174	1.75	10	[12]

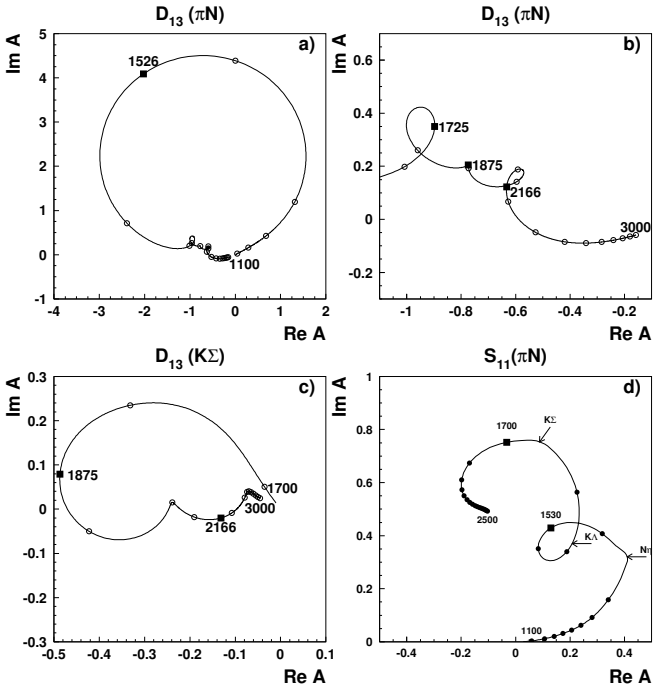

Fig. 1. a) Argand diagram for the $\gamma p \to p\pi$ D_{13} amplitude with helicity 3/2 from [8]. Data were fitted with the sum of four D_{13} multi-channel Breit-Wigner amplitudes. b) Enlarged view of the high-mass region. c) The amplitude for $\gamma p \to \Sigma K$ reveals contributions from higher-mass states. d) S_{11} from the SAID data base [22]. The units in d) are correct, those in a),b),c) have to be multiplied by 0.01.

complete information on polarization variables, etc.) make this approach so far impossible, in particular, when large orbital angular momenta are to be included. This approach abstains from using the analytic constraints provided by the S-matrix. Models, respecting carefully the analytic constraints, have a much closer contact to the physics we are aiming at. Polarization variables are then exploited not to construct but to constrain amplitudes used to describe the data.

A very important information carried by a scattering amplitude is its phase. In this paper we suggest a technique how the phase motion of a resonance can be visualized. The observation of a sizeable phase motion in a partial wave using this technique demonstrates consistency of the data with the observation of a resonance.

2 Phase motion of baryon resonances

2.1 The scanning technique

Figure 1 shows the basic idea of the new technique. The Argand diagram in fig. 1a for the helicity 3/2 $\gamma p \to p\pi$ D_{13} amplitude $A^{\frac{3}{2}}$ (determined in [8]) reveals a big circle due to $N(1520)D_{13}$. Its radius defines the product $g_{\gamma p} g_{N\pi}/\Gamma_{\rm tot}$ (see eq. (2)). The high-mass region is shown enlarged in fig. 1b. Three rather small epicycles are found by the fit which would be hard to see when the elastic amplitude is reconstructed from data. When the $N(1520)D_{13}$ resonance is described, the residual amplitude still exhibits loops due to the additional resonances. The higher-mass D_{13} resonances have small photocouplings, $N(1870)D_{13}$ also a small elastic width. The latter amplitude is better seen in $\gamma p \to \Sigma K$, see fig. 1c where $N(1870)D_{13}$ provides a significant contribution. A simultaneous search for D_{13} resonances in several final states will identify the most significant phase motion. For isobars with small or without resonant structure, the coupling will be fitted to a small value or to zero.

A more difficult example is given by the S_{11} partial waves. The Argand diagram in fig. 1d shows the elastic scattering amplitude from the SAID fit to the model-independent partial-wave analysis [22]. It presents —as far as we know— the worst case: the $N(1535)S_{11}$ and $N(1650)S_{11}$ resonances have strong couplings to $N\eta$, ΛK and ΣK channels which open in the central parts of the resonances. No angular momentum barrier prevents the decays, hence inelasticities lead to sharp variations of the amplitudes. At the opening of new channels, the curvature changes rapidly which may lead to wrong claims of additional resonances. Such a behavior is not expected at high masses, above 1.8 GeV; many decay modes are open and the opening of an additional channel has less significant consequences. Also, additional channels which open in this mass range like $\Delta(1232)\omega$ or $N(1680)F_{15}\pi$ have a soft threshold behavior, and sudden changes of the phase are unlikely.

In the isobar model fit presented in [8] most resonances (with mass M) were described by Breit-Wigner amplitudes with mass-dependent widths $\Gamma_{\rm tot}(s)$ where $g_{\gamma N}(s)$ and $g(s)$ define the couplings of the resonance to the initial and the final state at $s = M^2_{\gamma N}$.

$$A = \frac{g_{\gamma N}(s) g(s) e^{i\varphi}}{M^2 - s - i\, M \Gamma_{\rm tot}(s)}\,. \qquad (2)$$

In a quark model without hadronic rescattering taken into account, the phases φ are expected to vanish. Rescattering effects may however lead to non-zero phases. The phases are therefore allowed to deviate from zero in fits to mimic rescattering effects. Possible changes of the moduli are absorbed in the coupling constants. In πN scattering, both coupling constants would be given by the πN coupling constant $g_{\pi N}$ of the resonance. Due to the smallness of $g_{\gamma N}$, the amplitude does not follow a unitarity circle. However, as long as no important new thresholds open in close vicinity of the resonance, the amplitude carries the full phase motion of a resonance. The phase can be determined by interference with other amplitudes. The initial and final state are defined experimentally; a large number of amplitudes contribute. Most of these amplitudes interfere with the resonant amplitude under study. When the phase of the resonance is determined relative to another fixed amplitude, then the phase motion should become visible.

Figure 2 shows the squared amplitude and the phase of a model N(1520)D_{13} resonance. Its mass is 1520 MeV, its width 120 MeV, it is supposed to couple with 50% to Nπ and with 50% to N$\pi\pi$. A fit using a simple one-channel Breit-Wigner amplitude of fixed width will optimize the mass of the resonance and the overall phase. If a wrong mass is enforced by the fit, the fit quality (in terms of χ^2) decreases, the amplitude decreases but the fit can be improved by adding an overall phase shift $\delta\varphi$ as to reproduce the phase of the resonance where the overlap of true resonance and shifted resonance is large (see fig. 2). Far below (above) the peak position, the phase of the physical amplitude is close to zero (180°). If we test the amplitude with an artificial resonance peaking far below (above) the peak position of the physical amplitude, the artificial Breit-Wigner has not only a wrong amplitude but also a wrong phase. This can be compensated by adding a phase of −90° (+90°). When the resonance is stepped through in a mass scan, the added phase changes continuously from −90° to 90°. The mass scan can be simulated by using —instead of the data— a theoretical Breit-Wigner amplitude with parameters as derived in the fit. We call the resulting phase the *simulated phase motion*.

This technique to visualize the phase motion of hadronic resonances was first tested in the PhD Thesis of B. Pick [23] to explore the spectrum of ρ radial excitations in their $\omega\pi$ decay mode. Data of the Crystal Barrel Collaboration on the reaction $\bar{\rm p}{\rm n} \to \omega\pi^-\pi^0$ were used in that analysis.

2.2 The baryon phase motion from Breit-Wigner scans

We test these ideas by a discussion of the N(1680)F_{15} phase motion. This resonance couples strongly to Nγ and it is isolated, the next resonance in the F_{15} partial wave being expected to have a mass of about 2 GeV.

The full data set described above is fitted, all masses, widths and coupling constants are allowed to vary freely. The fit converges with χ^2 values as given in table 1. We now change the N(1680)F_{15} mass to preselected values keeping its width fixed. All other parameters can change again in a new fit. The $\chi^2_{\rm tot}$ of the fit deteriorates, when the N(1680)F_{15} mass is changed in steps. The change in $\chi^2_{\rm tot}$ as a function of the imposed N(1680)F_{15} mass is plotted in fig. 3a. A clear minimum is seen which determines the best N(1680)D_{13} parameters for those data. The phase φ resulting from the fit is shown in fig. 3b and compared to the expected phase motion. The change in the overall phase across the resonance is about 150° and reasonably close to the simulated phase motion. The errors in the fits,

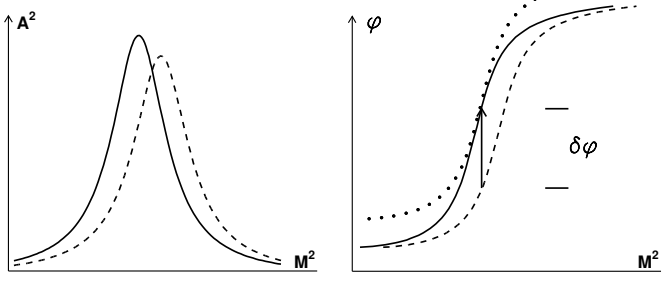

Fig. 2. Squared amplitude (left) and phase (right) of a model N(1520)D_{13} resonance according to eq. (2) (solid line). If the mass of the N(1520)D_{13} resonance is forced to be 1580 MeV, the fit will have a larger χ^2 and will return a smaller amplitude and a shifted phase (dashed line). The phase motions of the original resonance and of the shifted resonance can be made to agree in the mass region of largest intensity by adding a constant phase shift to the shifted resonance (dotted line).

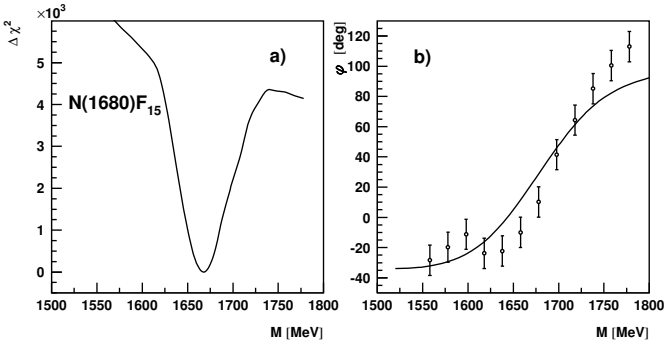

Fig. 3. a) Change in fit quality $\Delta\chi^2_{\rm tot}$ as a function of the imposed mass of the N(1680)F_{15} resonance. The minimum corresponds to the best solution with χ^2's as given in table 1. b) The phase φ adjusts itself to map the phase motion of the N(1520)D_{13} resonance. The phases determined by the fit are given as data points; they are compared to the simulated phase motion (see text) represented by the solid line.

$\pm 10°$, represent an educated guess. The statistical errors are always below 1° but they are highly correlated; the same data are used for all fits.

One could argue that the phase variation is a bias of the fit procedure. A local minimum was reached in the final fit which included the Breit-Wigner amplitude. Replacing this amplitude by another similar amplitude may lead automatically to the expected phase variation. This argument may be true in some cases but proved to be wrong in at least this case: the technique was also applied to study the reaction $\bar{p}p \to 2\pi^+2\pi^-\eta$. The likelihood fit identifies two resonances, $\eta(1405)$ and $\eta(1475)$, both decaying to the final state via $\sigma\eta$ and $a_0(980)\pi$. Mass and widths of these two resonances were determined to $M = (1407 \pm 5)\,\mathrm{MeV}$, $\Gamma = (57 \pm 9)\,\mathrm{MeV}$ and $M = (1490 \pm 25, \Gamma = 80 \pm 25)$ MeV, respectively. Thus the two resonances are sufficiently separated to expect at least partly separated phase motions. However, the phase of the $\pi^+\pi^-\eta$ pseudoscalar partial wave changed by only 180° in the mass range from 1300 to 1500 MeV [24] (and not by more than 300° as one should expect if $\eta(1405)$ and $\eta(1475)$ would be two independent particles [25]). At least in this case, the phase motion gives an answer which is different from the conclusion drawn by likelihood fitting.

We test the technique in three applications discussed in some detail below. First, we reduce the model space to an absolute minimum. Second we replace the K-matrix for the two S_{11} amplitudes by two multi-channel Breit-Wigner amplitudes. And then we test the $N(1520)D_{13}$ resonance which makes a very large contribution to the $\gamma p \to p\pi^0$ total cross-section.

The minimal model

We reduce the model space to a few components only, and restrict to amplitudes representing the 3 resonance regions by $\Delta(1232)$, $N(1520)D_{13}$ and $N(1680)F_{15}$, and to t- and u-channel exchange amplitudes to take into account the background. This test is intended to examine if the phase motion is picked up correctly even in the case of an incomplete model. The χ^2 of the fit is now $132.5 \cdot 10^3$ instead of $12.5 \cdot 10^3$ for the best fit. Obviously the fit describes only the gross features of the data. Nevertheless, a clear χ^2 minimum and a strong phase motion is observed in fig. 4, both at the expected mass. The phase motion is stronger than predicted. Of course, we cannot assign minimum and phase motion to $N(1680)F_{15}$ production only; other resonances in the third resonance region may contribute as well.

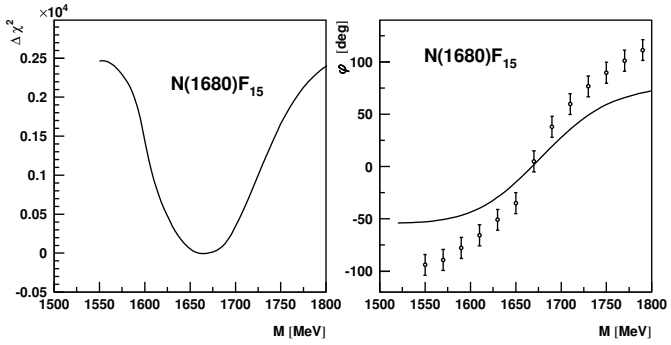

Fig. 4. $\Delta\chi^2_{\mathrm{tot}}$ as a function of the imposed $N(1680)F_{15}$ mass and its phase φ in a minimal model with very few amplitudes. Apart from t- and u-channel exchange amplitudes, only three resonances are used to describe the data, $\Delta(1232)$, $N(1520)D_{13}$ and the F_{15} wave with variable mass.

The two S_{11} resonances

As a next step, we fit the S_{11} wave by replacing the K-matrix by two multi-channel Breit-Wigner amplitudes. The $N(1535)S_{11}$ is used with free parameters, the $N(1650)S_{11}$ mass is scanned. The results are shown in fig. 5. Even under these unfavorable circumstances, with thresholds of two channels strongly coupling to the S_{11} wave, the expected phase motion is clearly observed.

The D_{13} resonances

We expected also a clear phase motion for the D_{13} partial wave but these expectations are only partly met as demonstrated in fig. 6. The region of the most rapid phase motion is found ~ 70 MeV above its nominal mass. This is

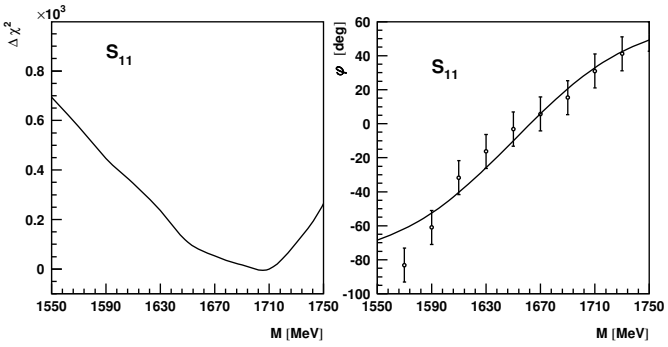

Fig. 5. $\Delta\chi^2_{\mathrm{tot}}$ as a function of the imposed $N(1650)S_{11}$ mass and its phase φ. See the caption of fig. 3 for further details.

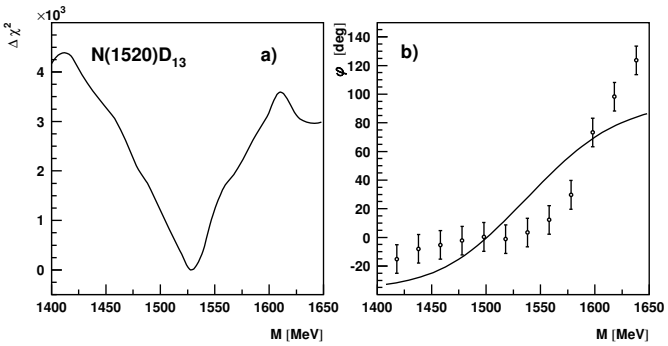

Fig. 6. Change in fit quality $\Delta\chi^2_{\mathrm{tot}}$ as a function of the imposed $D_{13}(1520)$ mass and its phase. See the caption of fig. 3 for further details.

a problem intrinsic in this technique if strongly contributing resonances are investigated. When a wrong mass of a strong resonance is enforced, the χ^2 changes very significantly. A new fit minimum can then be found which is no longer similar to the best solution. For a large mismatch between the imposed and true mass of the resonance, the fit is hence no longer capable to reproduce the phase accurately. The technique is thus best suited for resonances with moderate contributions to the data.

2.3 The newly proposed resonances

We next test the resonant behavior of the four newly proposed resonances, $N(1840)P_{11}$, $N(1870)D_{13}$, $N(2070)$ D_{15} and $N(2170)D_{13}$. The results are presented in fig. 7. In all cases, the phase variation exceeds 120° and follows the simulated phase motion.

We now comment on the individual graphs in fig. 7. The $N(1840)P_{11}$ exhibits, like the $N(1680)F_{15}$ resonance, a nearly ideal case: there is a clear $\chi^2_{\rm tot}$ minimum and the observed $N(1840)P_{11}$ phase resonance follows almost exactly the simulated phase motion. The same statement can be made for the $N(2070)D_{15}$. The D_{13} resonances are much more difficult. There are four of them, and in the mass scan interfering Breit-Wigner amplitudes are offered to the fit, which start to overlap strongly when the scanned mass approaches one of the neighboring D_{13} resonances. This leads to instabilities in the fit. The minimum of the $N(1870)D_{13}$ resonance is very asymmetric and the mass is difficult to determine from this plot. Here it is necessary to recall that the $N(1870)D_{13}$ parameters were determined from a $N(1870)D_{13}$ $\chi^2_{\rm tot}$ scan of the fit to the ΛK^+ and ΣK data, where a clear minimum evolved. The overall fit is not necessarily the optimal choice to determine parameters of a resonance with strong couplings to a rare decay mode. We interprete the $\chi^2_{\rm tot}$ plot in fig. 7 as evidence that the $N(1870)D_{13}$ starts to interfere with $N(1700)D_{13}$ on the low-mass side and with $N(2170)D_{13}$ on the high-mass side. Likewise, the overall $\chi^2_{\rm tot}$ scan (summed over all data in table 1) in fig. 7 does not give a reliable measure of the presence of $N(2170)D_{13}$. But the phase motion is not strongly distorted by these problems and seems to provide stronger evidence for the existence of the two new D_{13} resonances than the $\chi^2_{\rm tot}$ distributions.

Next we explore if the technique proposed here is sensitive to the quantum numbers of a resonance. We describe $N(2070)D_{15}$ with spin $(7/2)^-$. The $\chi^2_{\rm tot}$ distribution and the phase motion resulting from this hypothesis are shown in fig. 8. The $\chi^2_{\rm tot}$ as a function of the assumed G_{17} mass exhibits a double structure, one of the minima is incompatible with the mass deduced from the phase motion while the phase has not changed significantly. The likelihood hardly discriminates the two solutions yielding different mass values. The phase motion certainly supports only one solution. Both solutions give a reasonable likelihood even though the angular momentum J is wrong. In this case (and other cases considered), a correct phase motion is obviously a stronger indicator for the resonance parameters than the angular distribution.

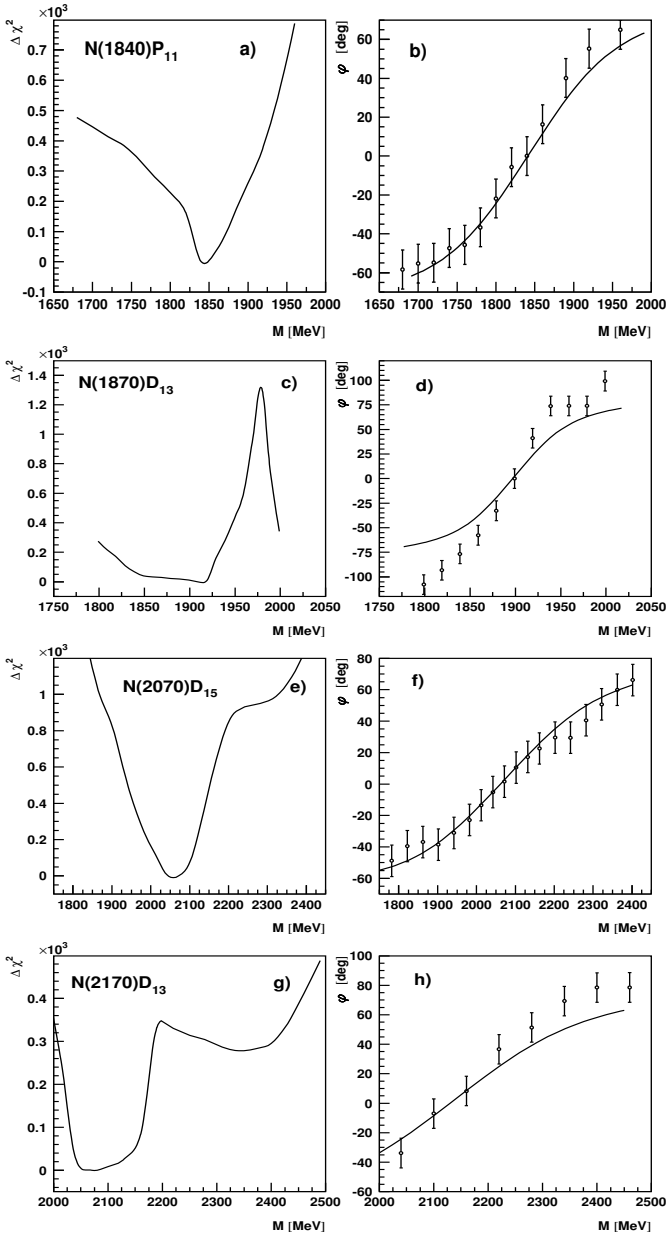

Fig. 7. $\Delta\chi^2_{\rm tot}$ as a function of the imposed $N(1840)P_{11}$ (a), $N(1870)D_{13}$ (c), $N(2070)D_{15}$ (e), and $N(2170)D_{13}$ (g) mass, and their respective phases φ (b, d, f, h). See caption of fig. 3 for further details.

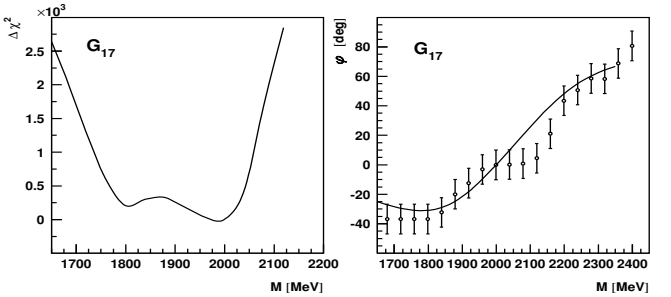

Fig. 8. $\Delta\chi^2_{\rm tot}$ and the phase φ as a function of the imposed mass when $N(2070)D_{15}$ is replaced by a G_{17} amplitude. See the caption of fig. 3 for further details.

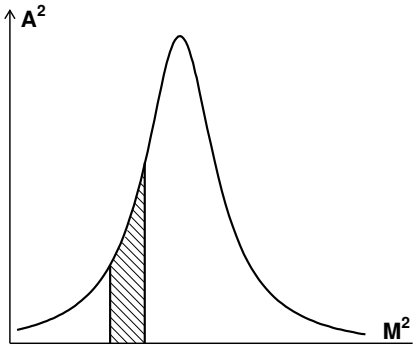

Fig. 9. In the slice technique to determine the phase motion, a baryon resonance is described by a Breit-Wigner amplitude. In a mass slice, the amplitude can adopt an arbitrary additional phase φ.

2.4 The slice technique

Finally, we try another technique to explore the phase motion of a resonance. The technique is explained in fig. 9. A slice in the mass spectrum of a Breit-Wigner amplitude is multiplied with $\exp(i\varphi)$ where φ is an arbitrary number. Otherwise, the Breit-Wigner amplitude remains unchanged. (The fit may however change mass, width, strength and overall phase.)

2.5 The baryon phase motion from mass slices

We first test the technique using the well-known $N(1520)D_{13}$ and $N(1680)F_{15}$ resonances. The resulting phases are shown in fig. 10.

The phases in the mass slices follow closely the expected Breit-Wigner phase motion, a mean deviation of less than 3.5° is derived from fig. 10. Obviously, interference effects play a very important role and define sharply the phase of a baryon resonance. Next, we apply the slice technique to the $N(2070)D_{15}$. At the same time we test the sensitivity of the slice technique to quantum numbers of baryon resonances. The results are shown in fig. 11.

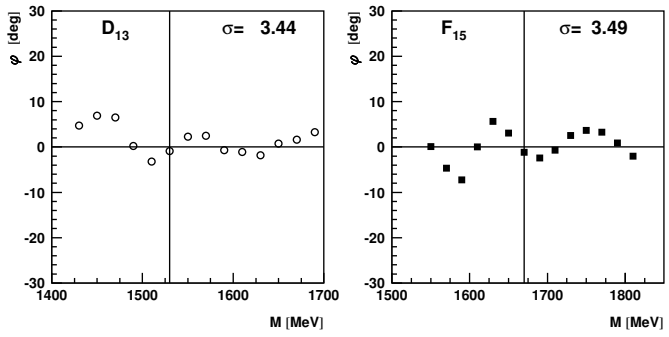

Fig. 10. The phase difference φ between the Breit-Wigner phase and the phase fitted in a mass slice as a function of the mass. See the caption of fig. 9 for further explanations.

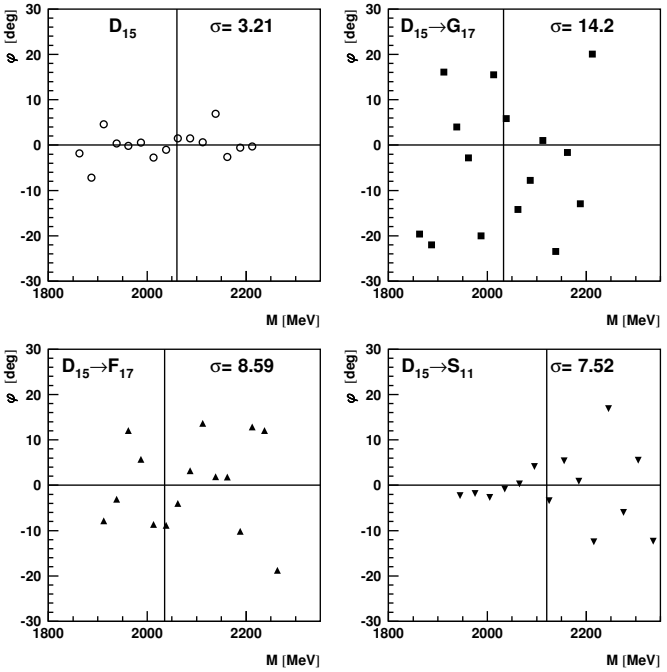

Fig. 11. The additional phase φ (in degrees) which is allowed to vary freely in a selected mass slice. The fit had assigned D_{15} quantum numbers to the resonance. The local phase deviates only weakly (with a spread $\sigma = 3.21°$) from the expected Breit-Wigner phase. When the quantum numbers of the additional resonance are changed the additional phase still follows a Breit-Wigner amplitude but the mean deviations between expected and fitted phase increase.

The D_{15} amplitude gives very good agreement between fitted and expected phase over the full mass range (upper left plot). A replacement by a G_{17}, F_{17} or S_{11} amplitude introduces a much larger variance; obviously a D_{15} amplitude is best suited to describe the data while the phases become less stable when other quantum numbers are tested.

3 Summary and outlook

A novel technique is proposed to visualizes the phase motion of hadron resonances. The technique exploits the freedom of a fit to adjust the overall phase of a Breit-Wigner amplitude independently of its mass. The phase motions of the established resonances like $N(1520)D_{13}$, $N(1535)S_{11}$ and $N(1680)F_{15}$ resonances are used to verify the validity of the technique. The newly proposed resonances, $N(1840)\ P_{11}$, $N(1870)D_{13}$, $N(2070)D_{15}$, and $N(2170)\ D_{13}$, are shown to exhibit the expected phase motion, too. Thus the evidence for the existence of these states finds additional support.

The technique is not comparable with a determination of the phase in a model-independent reconstruction of the amplitude. But it offers the possibility of an important consistency check: we have found at least one example in which a likelihood fit gives strong support for two reso-

nances while the phase scan gives only one. The method seems to be stable against moderate model errors, wrong hypotheses may result in inconsistencies between mass values found in a likelihood scan and in the deduced phase motion. Further work is certainly needed to establish the reliability and the limit of this new technique.

Are further polarization data still required to establish these resonances ? Certainly yes. New data on single- and double-polarization variables will provide further constraints, lead to larger $\chi^2_{\rm tot}$ differences when resonances are introduced and will hopefully uncover the existence of further baryon resonances with weaker couplings to the γp initial state.

We would like to thank the CB-ELSA/TAPS Collaboration for numerous discussions on topics related to this work. We acknowledge financial support from the Deutsche Forschungsgemeinschaft within the SFB/TR16. The St. Petersburg group received funds from the Russian Foundation for Basic Research (grant 04-02-17091). U.T. thanks for an Emmy Noether grant from the DFG. A.A. and A.S. acknowledge generous support by the Alexander von Humboldt foundation in the initial phase of the project.

References

1. S. Capstick, N. Isgur, Phys. Rev. D **34**, 2809 (1986); S. Capstick, W. Roberts, Prog. Part. Nucl. Phys. **45**, S241 (2000); Phys. Rev. D **58**, 074011 (1998).
2. L.Y. Glozman, W. Plessas, K. Varga, R.F. Wagenbrunn, Phys. Rev. D **58**, 094030 (1998).
3. U. Löring, K. Kretzschmar, B.C. Metsch, H.R. Petry, Eur. Phys. J. A **10**, 309 (2001); U. Löring, B.C. Metsch, H.R. Petry, Eur. Phys. J. A **10**, 395, 447 (2001).
4. E. Klempt, *Baryon resonances and strong QCD*, arXiv:nucl-ex/0203002; Phys. Rev. C **66**, 058201 (2002).
5. V.D. Burkert, R. De Vita, M. Battaglieri, M. Ripani, V. Mokeev, Phys. Rev. C **67**, 035204 (2003).
6. L.Y. Glozman, Phys. Lett. B **475**, 329 (2000).
7. E. Klempt, Phys. Lett. B **559**, 144 (2003).
8. A.V. Anisovich, A. Sarantsev, O. Bartholomy, E. Klempt, V.A. Nikonov, U. Thoma, Eur. Phys. J. A **25**, 427 (2005); A. Sarantsev, V.A. Nikonov, A.V. Anisovich, E. Klempt, U. Thoma, Eur. Phys. J. A **25**, 441 (2005).
9. O. Bartholomy *et al.*, Phys. Rev. Lett. **94**, 012003 (2005).
10. V. Crede *et al.*, Phys. Rev. Lett. **94**, 012004 (2005).
11. B. Krusche *et al.*, Phys. Rev. Lett. **74**, 3736 (1995).
12. O. Bartalini *et al.*, Eur. Phys. J. A **26**, 399 (2005).
13. A.A. Belyaev *et al.*, Nucl. Phys. B **213**, 201 (1983); R. Beck *et al.*, Phys. Rev. Lett. **78**, 606 (1997); D. Rebreyend *et al.*, Nucl. Phys. A **663**, 436 (2000).
14. J. Ajaka *et al.*, Phys. Rev. Lett. **81**, 1797 (1998).
15. K.H. Althoff *et al.*, Z. Phys. C **18**, 199 (1983); E.J. Durwen, BONN-IR-80-7 (1980); K. Buechler *et al.*, Nucl. Phys. A **570**, 580 (1994).
16. K.H. Glander *et al.*, Eur. Phys. J. A **19**, 251 (2004).
17. R. Lawall *et al.*, Eur. Phys. J. A **24**, 275 (2005).
18. J.W.C. McNabb *et al.*, Phys. Rev. C **69**, 042201 (2004).
19. B. Carnahan, *Strangeness photoproduction in the* γp $\rightarrow$ $K^0\Sigma^+$ *reaction*, UMI-31-09682 (microfiche), PhD Thesis, at the Catholic University of America, Washington, D.C. (2003).
20. R.G.T. Zegers *et al.*, Phys. Rev. Lett. **91**, 092001 (2003).
21. A. Anisovich, E. Klempt, A. Sarantsev, U. Thoma, Eur. Phys. J. A **24**, 111 (2005).
22. R.A. Arndt *et al.*, `http://gwdac.phys.gwu.edu`.
23. Crystal Barrel Collaboration (C. Amsler *et al.*), Nucl. Phys. A **740**, 130 (2004).
24. E. Klempt, *The glueball candidate* $\eta(1440)$ *as* η *radial excitation*, arXiv:hep-ph/0409148.
25. Particle Data Group Collaboration (S. Eidelman *et al.*), Phys. Lett. B **592**, 1 (2004).